The Astrophysical Journal Letters, 818:L3 (6pp), 2016 February 10 doi:10.3847/2041-8205/818/1/L3

FIRST OBSERVATIONAL SUPPORT FOR OVERLAPPING REIONIZED BUBBLES GENERATED BY A GALAXY OVERDENSITY

M. Castellano[1], P. Dayal[2,3], L. Pentericci[1], A. Fontana[1], A. Hutter[4], G. Brammer[5], E. Merlin[1], A. Grazian[1], S. Pilo[1], R. Amorin[1], S. Cristiani[6,7], M. Dickinson[8], A. Ferrara[9], S. Gallerani[9], E. Giallongo[1], M. Giavalisco[10], L. Guaita[1], A. Koekemoer[5], R. Maiolino[11,12], D. Paris[1], P. Santini[1], L. Vallini[9,13], E. Vanzella[14], and J. Wagg[15]
[1] INAF—Osservatorio Astronomico di Roma, Via Frascati 33, I-00040 Monte Porzio Catone (RM), Italy; marco.castellano@oa-roma.inaf.it
[2] Institute for Computational Cosmology, Department of Physics, University of Durham, South Road, Durham DH1 3LE, UK
[3] Kapteyn Astronomical Institute, University of Groningen, P.O. Box 800, 9700, AV Groningen, The Netherlands
[4] Swinburne University of Technology, Hawthorn, VIC 3122, Australia
[5] Space Telescope Science Institute, 3700 San Martin Drive, Baltimore, MD 21218, USA
[6] INAF—Osservatorio Astronomico di Trieste, Via G. B. Tiepolo 11, I-34143 Trieste, Italy
[7] INFN—National Institute for Nuclear Physics, via Valerio 2, I-34127, Trieste, Italy
[8] National Optical Astronomy Observatories, Tucson, AZ 85719, USA
[9] Scuola Normale Superiore, Piazza dei Cavalieri 7, I-56126 Pisa, Italy
[10] Astronomy Department, University of Massachusetts, Amherst, MA 01003, USA
[11] Cavendish Laboratory, University of Cambridge, 19 J. J. Thomson Avenue, Cambridge CB3 0HE, UK
[12] Kavli Institute for Cosmology, University of Cambridge, Madingley Road, Cambridge CB3 0HA, UK
[13] Dipartimento di Fisica e Astronomia, Università di Bologna, viale Berti Pichat 6/2, I-40127 Bologna, Italy
[14] INAF—Osservatorio Astronomico di Bologna, Via Ranzani 1, I-40127, Bologna, Italy
[15] Square Kilometre Array Organization, Jodrell Bank Observatory, Lower Withington, Macclesfield, Cheshire SK11 9DL, UK
Received 2015 December 21; accepted 2016 January 13; published 2016 February 1

ABSTRACT

We present an analysis of deep *Hubble Space Telescope* (*HST*) multi-band imaging of the BDF field specifically designed to identify faint companions around two of the few Lyα emitting galaxies spectroscopically confirmed at $z \sim 7$. Although separated by only 4.4 proper Mpc these galaxies cannot generate H II regions large enough to explain the visibility of their Lyα lines, thus requiring a population of fainter ionizing sources in their vicinity. We use deep *HST* and VLT-Hawk-I data to select $z \sim 7$ Lyman break galaxies around the emitters. We select six new robust $z \sim 7$ LBGs at $Y \sim 26.5$–27.5 whose average spectral energy distribution is consistent with the objects being at the redshift of the close-by Lyα emitters. The resulting number density of $z \sim 7$ LBGs in the BDF field is a factor of approximately three to four higher than expected in random pointings of the same size. We compare these findings with cosmological hydrodynamic plus radiative transfer simulations of a universe with a half neutral IGM: we find that indeed Lyα emitter pairs are only found in completely ionized regions characterized by significant LBG overdensities. Our findings match the theoretical prediction that the first ionization fronts are generated within significant galaxy overdensities and support a scenario where faint, "normal" star-forming galaxies are responsible for reionization.

Key words: dark ages, reionization, first stars – galaxies: high-redshift

1. INTRODUCTION

In recent years, spectroscopic follow-up campaigns of $z \sim 7$ Lyman break galaxies (LBGs) have enabled a direct investigation of the timeline of the reionization process by studying the redshift evolution of the Lyα fraction in LBGs (Stark et al. 2010), which is expected to fall-off when the IGM becomes significantly neutral and Lyα emission is attenuated (Dijkstra 2016). A substantial decrease of the Lyα fraction between $z \sim 6$ and $z \sim 7$ has been measured (Fontana et al. 2010; Pentericci et al. 2011; Caruana et al. 2012; Ono et al. 2012; Schenker et al. 2012), with the latest data favoring a scenario with a change of the neutral hydrogen fraction of $\Delta\chi_{\rm H\,I} \sim 0.5$ in a redshift interval $\Delta z = 1$, and a patchy reionization process (Treu et al. 2012; Pentericci et al. 2014). Bouwens et al. (2015a) have shown that, under plausible assumptions of the properties of star-forming galaxies, the evolution of their UV luminosity density can explain the reionization timeline estimated from spectroscopic data and other probes. However, significant uncertainties remain: direct evidence of the connection between galaxies and reionization as well as an explanation of the patchiness found from spectroscopy are still missing. Among the eight independent lines of sight analyzed by Pentericci et al. (2014), the Bremer Deep Field (BDF) stands out as a peculiar area in the $z \sim 7$ universe. The BDF is the only field where two close-by bright Lyα-emitting galaxies, BDF-3299 ($z = 7.109$) and BDF-521 ($z = 7.008$) have been found (Vanzella et al. 2011). These two $L \sim L^*$ objects, originally selected as z-dropout candidates (Castellano et al. 2010b, C10b hereafter), show Lyα equivalent widths > 50 Å and are separated by a distance of only 4.4 proper Mpc (pMpc). The detection of bright Lyα emission from these objects can be explained by these sources being embedded in an H II region that allows Lyα photons to redshift far away from the line center before they reach the almost neutral IGM. Vanzella et al. (2011) has compared the size of the H II region these galaxies can build (Loeb et al. 2005) to the minimum ionized radius, allowing their Lyα photons to escape (Wyithe & Loeb 2005), finding that they both cannot generate H II regions large enough to explain the visibility of their lines even if a maximum Lyman continuum escape fraction $f_{\rm esc} = 1$ is assumed. Instead, the visibility of their Lyα can be explained by the presence of additional ionizing sources in their vicinity (Dayal et al. 2009). Unfortunately, the data available at that time did not allow us to select galaxies fainter than the two

emitters to constrain this hypothesis. In this paper, we present the analysis of deep *Hubble Space Telescope* (*HST*) observations of the BDF region (cycle 22 program 13688, P.I. M. Castellano) specifically designed to detect possible fainter companions of BDF-3299 and BDF-521. Throughout the paper, magnitudes are in the AB system, and we adopt the Λ-CDM concordance model ($H_0 = 70$ km s^{-1} Mpc^{-1}, $\Omega_M = 0.3$, and $\Omega_\Lambda = 0.7$).

2. DATA SET AND $z \sim 7$ LBG SELECTION

The *HST* observations of the BDF field consist of two pointings including BDF-3299 and BDF-521 and are designed to cover the largest possible portion of the region between them. Each pointing has been observed with WFC3 in the Y105 filter (three orbits) and with ACS filters I814 (three orbits) and V606 (two orbits). The *HST* images were processed as described in detail by Momcheva et al. (2015), taking into account time-variable backgrounds and high-altitude atmospheric line emission (Brammer et al. 2014). The individual exposures in each band were registered and combined with `DrizzlePac` (Gonzaga et al. 2012) into mosaics with 0.06 arcsec pixel scales. Coverage redward of the Y105 band is needed to separate LBGs from low-redshift red interlopers. To this aim, we exploit the *J*- and *K*-band HAWK-I data (C10b) to build a $J + K$ mosaic as the weighted average of the two data sets after having matched the *K* band PSF to the *J* band one. We include in the analysis our reduction of the J125 and H160 observations of the BDF-521 field acquired under program 12487 (PI X. Fan, Cai et al. 2015) that partially overlap with our Y105 data. We detect sources in the Y105 band with `SExtractor` (Bertin & Arnouts 1996) and use the relevant `FLUX_AUTO` value as total flux in this band. We PSF-match the other *HST* bands to the Y105 one through appropriate convolution kernels and then use `SExtractor` in dual-mode to obtain total magnitudes in each band by scaling total Y105 flux on the basis of the relevant isophotal color. To measure photometry from the $J + K$ mosaic whose resolution (0.55 arcsec PSF FWHM) is signficantly lower than the Y105 one (0.19 arcsec), we perform double-pass `T-PHOT` runs using source cutouts from the Y105 image as reference high-resolution templates (Merlin et al. 2015).

The resulting magnitude limits in 2 × FWHM apertures are: V606 = 30.6, I814 = 30.4, (S/N = 1), Y105 = 28.0 (S/N = 10), $(J + K) = 27.6$ (S/N = 1).

We use templates from the Bruzual & Charlot (2003; BC03 hereafter) library including both high- and low-z galaxies to define the following LBG selection window (Figure 1):

$$(\mathrm{S/N}(I_{814}) < 1) \wedge (I_{814} - Y_{105} > 2.2)$$
$$Y_{105} - (J + K) < 0.8$$
$$(\mathrm{S/N}(Y_{105}) > 10) \wedge (\mathrm{S/N}(V_{606})) < 1,$$

where the signal-to-noise ratio (S/N) in the Y105 band is associated with the total flux and relevant uncertainty in this band, and S/Ns in the ACS bands are measured in 2 × FWHM apertures. The strict non-detection in the I814 band, plus the requirement on I814-Y105 > 2.2 (that is met at $z > 6.5$) ensures that we are selecting objects in the standard z-dropout redshift range. We also apply additional criteria to include only objects with robust photometry. These have been defined with the procedure outlined in Castellano et al. (2010a) based on the analysis of a "negative" detection image, ensuring that no spurious detections are expected for S/N(Y105) > 10 samples. To avoid noisy areas, we retrict the analysis to regions where the rms of the images is less than ∼1.5 times the lowest value. The resulting total area used for the analysis is 3.94 and 3.82 sq. arcmin in the BDF-521 and BDF-3299 pointings respectively. We also require an optimal `SExtractor` extraction flag (`FLAG` = 0), and an isophotal area `ISOAREA` > 18 pixels (equal to two times the area of one FWHM of the Y105 PSF) to avoid detections possibly due to residual cosmic-rays or hot pixels.

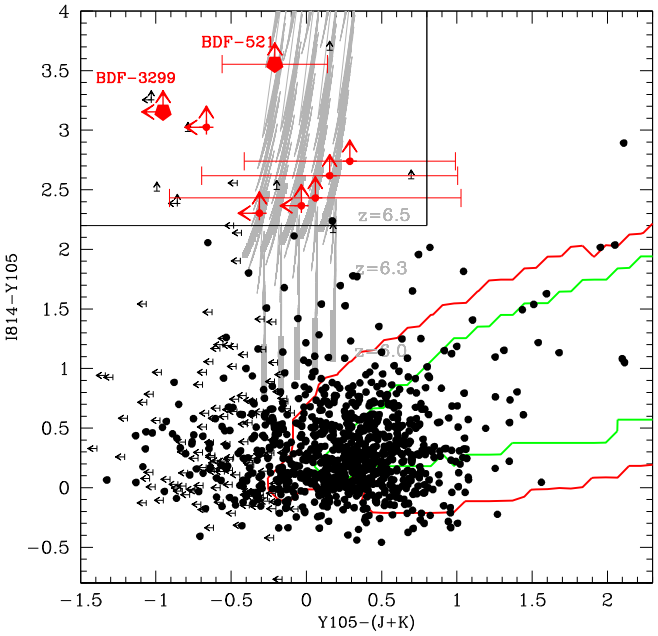

Figure 1. I814-Y105 vs. Y105-($J + K$) diagram of the objects in the *HST*-BDF catalogs. The $z \sim 7$ LBG selection region is enclosed by the box: the selected candidates are marked in red, with BDF-521 and BDF-3299 indicated by filled pentagons. Gray lines show the position of star-forming BC03 models at $z > 6.0$ (see labels) with $0.0 < E(B - V) < 0.2$ (from left to right), age = 100 Myr, constant SFH, $Z = 0.2Z_\odot$. Red and green contours show, respectively, the position of passive and dusty BC03 templates at $z < 4$.

Our selection criteria yield four LBG candidates in each BDF pointing (Figure 1). Reassuringly, both BDF-521 and BDF-3299 are included in our selected sample together with six additional LBGs at Y105 ∼ 26.5–27.5. Among the six newly discovered LBGs, three sources show a marginal detection in the ($J + K$) mosaic at S/N ∼ 1–1.5. Two of the sources in the BDF-521 pointing (one of them undetected in $J + K$) are also included in the area of the WFC3 observations from Cai et al. (2015) and are detected at S/N ∼ 2–8 in both the J125 and H160 bands with colors expected for $z \sim 7$ LBGs. All of our BDF candidates are extended with half-light radii in the range Rh ∼ 0.09–0.17 arcsec, consistent with expectations for $z \sim 7$ galaxies in the same magnitude range (Grazian et al. 2012). In fact, they are classified with `CLASS_STAR` < 0.9 such that we can exclude that cool stars and transient objects contaminate our sample, since these kinds of contaminants are expected to have a higher stellarity index at S/N > 10 (Bouwens et al. 2015b). We compute the photometric redshift of the sources by fitting their photometry with our χ^2 minimization code (Fontana et al. 2000) using a library of BC03 templates at $z = 0$–8 (including line emission as in Schaerer & de Barros 2009; Castellano et al. 2014). We find

that all sources have best-fit solutions at high-z ($z \sim 6.8$–7.4) and are consistent, within the 1σ uncertainty, with the spectroscopic redshift of the two emitters.

2.1. Test of the LBG Selection Criteria on the HUDF

As a test of our selection criteria, we apply them to a real case by degrading HUDF V606, I814, Y105, J125, and Ks images (Koekemoer et al. 2013; Fontana et al. 2014) to the depth and resolution of the BDF data set. This is particularly interesting to test the efficiency of the $J + K$ data in separating red low-z interlopers (expected at $S/N \gtrsim 3$) from LBGs (close to the detection limit at $S/N = 1$). In practice, we add Gaussian noise to the V606, I814, Y105, and Ks images to match the depth of the BDF observations, and both smooth and decrease the depth of the J125 image to match the J-HAWKI mosaic of the BDF. We build a ($J + K$) mosaic and extract catalog and photometry in the same way as in the BDF case. Our selection criteria yield only one candidate: the LBG G2_1408 from Castellano et al. (2010a), well known in the literature, being selected by all analyses of the HUDF field (see Vanzella et al. 2014). The other $z \sim 7$ LBGs in the HUDF from Bouwens et al. (2015b) have Y105 $\gtrsim$ 27.7 (photometry from Guo et al. 2013) and are thus not expected as $S/N > 10$ sources in our data. Most importantly, we find that no $z < 6.5$ objects are scattered into our LBG selection window. In addition, no spurious detections are found, consistently with our finding from the "negative image" test.

2.2. Stacking of the Newly Identified LBGs

To further verify that the six newly discovered LBGs are genuine $z \sim 7$ sources, we build stacked (weighted average) images in the different bands enabling a tighter constraint on the Lyman break. We extract photometry from the stacked images with `SExtractor` and `T-PHOT`. We find non-detections in both the V606 and I814, corresponding to a limiting total magnitude >30.2 and to a color I814-Y105 > 3, and an $S/N \sim 2$ detection in the $J + K$ one. The stacked thumbnails and the resulting SED are shown in Figure 2. We find a best-fit photometric redshift $z = 6.95$, with $P(\chi^2) > 32\%$ solutions constrained to the range of $z = 6.8$–7.8, as expected from the sharp I814-Y105 drop. The spectroscopic redshifts of BDF-521 and BDF-3299 are close to the best-fit solution.

3. AN OVERDENSITY OF LBGs IN THE BDF

We use extensive simulations for a detailed assessment of the LBG number density observed in the BDF field, and in particular to compare it to expectations from our current knowledge of the $z \sim 7$ UV LF.

3.1. Expected Number Counts

We first generate a library of BC03 models at $6.0 < z < 8$, with constant SFH, age beween 10 Myr and the age of the universe at the relevant redshift, $0.0 < E(B - V) < 0.2$ (extinction law from Calzetti et al. 2000), and metallicities $Z = 0.02, 0.2, 1.0\ Z_{\odot}$. We randomly extract from it a reference catalog with 75,000 sources whose fluxes are renormalized so to follow a constant distribution at $-21.5 < M_{1500} < -18.5$. This catalog is used as input for simulations mimicking the survey properties. Observed magnitudes in the V606, I814, and Y105 bands are obtained by inserting mock galaxies in the real images and assembling the catalog as in the real case (see, e.g., C10b). We assume galaxy shapes to be disk-like with Rh randomly drawn from the distribution by Grazian et al. (2012). Imaging simulations are exceedingly time consuming in the case of `T-PHOT` photometry. We thus include $J + K$ "observed" magnitudes following the technique described in Castellano et al. (2012), namely we perturb the template fluxes through Monte Carlo simulations designed to reproduce both the average and the scatter of the (total) S/N versus magnitude relation in the observed $J + K$ data sets. We then randomly extract from our reference library galaxy populations following the latest estimates of the $z \sim 7$ UV LF from Bouwens et al. (2015b) and Finkelstein et al. (2015). We select objects in the same way as for the observed data sets and the resulting number counts are scaled to the observed area. Simulations and LBG selection are performed separately in the two pointings to take into account small differences in depth and coverage between them. We find that a total of $N_{\rm exp} = 1.8$–2.9 objects are expected in our *HST* survey of the BDF on the basis of the LFs from Finkelstein et al. (2015) and Bouwens et al. (2015b) respectively. The probability of detecting eight sources in our field out of a Poisson distribution with $N_{\rm exp} = 1.8$–2.9, is only 0.045%–0.68%, while the estimated cosmic variance[16] is $\sim 0.5 \cdot N_{\rm exp}$. This analysis confirms that the BDF field with its eight detected LBGs is a factor of approximately three to four overdense at $z \sim 7$ with respect to the average galaxy number density at these redshifts (Figure 3).

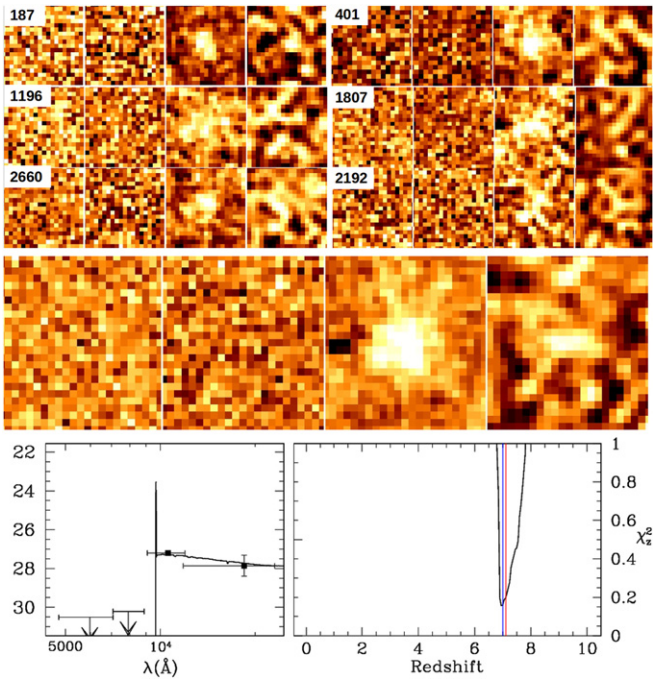

Figure 2. Top: thumbnails (1 arcsec side) of the newly detected LBGs in the BDF-521 (left column) and BDF-3299 (right column) *HST* pointings in, from left to right, V606, I814, Y105, and ($J + K$) bands. Middle: stacked thumbnails. Bottom: best-fit spectral energy distribution of the stacked object (left panel) and χ^2 as a function of redshift (right panel, red and blue lines mark the spectroscopic redshifts of BDF-3299 and BDF-521 respectively).

[16] Computed with the Cosmic Variance Calculator (Trenti & Stiavelli 2008), http://casa.colorado.edu/~trenti/CosmicVariance.html

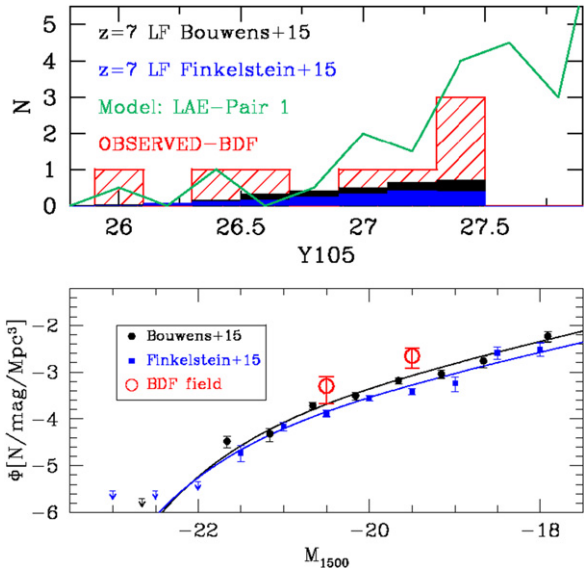

Figure 3. Top: observed number counts of $z \sim 7$ LBGs in the BDF field (red histogram) compared to the number counts expected from $z \sim 7$ LFs, and to number counts in the region of "Pair 1" in our cosmological simulations (green line). Bottom: stepwise $z \sim 7$ UV LF in the BDF field (red open circles) and the average one from wide surveys (Bouwens et al. 2015b; Finkelstein et al. 2015, black circles and blue squares respectively). The best-fit $z \sim 7$ LFs from Bouwens et al. (2015b) and Finkelstein et al. (2015) are shown as black and blue lines respectively.

3.2. Comoving Number Density

We recast our analysis into a comparison between the observed $z \sim 7$ LF in the BDF field and the average one from wide surveys. We perform a binned estimate of the comoving number density through a stepwise method (e.g., C10b). In practice, we assume the objects to be at $z = 7$ to convert Y-band magnitudes into M_{1500} rest-frame, and measure the number density in two bins as $N_{\rm obj}/V_{\rm eff}$, where $V_{\rm eff}$ is the effective volume probed by the survey at $z = 6.5$–7.5 as estimated from the simulations. The results are shown in the bottom panel of Figure 3 and confirm an excess of galaxies in the BDF field both at bright and faint magnitudes, although in the brightest bin (three sources) the BDF number density remains consistent with the LF by Bouwens et al. (2015b) within the Poissonian uncertainty. We underline that this is a conservative estimate since it has been obtained by considering the full effective volume probed by our survey. As an example, the real comoving number density in the BDF is ∼15 times higher than the average in case the six additional LBGs detected with *HST* data are physically associated with BDF-521 and BDF-3299 in a unique structure at $z \sim 7.1$ with $\Delta z = 0.25$.

4. DISCUSSION

The BDF field, showing both close-by emitters and a galaxy overdensity, displays all the properties of an early reionized region expected in theoretical models that postulate a dependence between galaxy density and the reionization timeline, with overdense regions being the first to become reionized "bubbles" (McQuinn et al. 2007; Wyithe & Loeb 2007; Dayal et al. 2009; Iliev et al. 2014). To test this scenario, we should eventually prove that the BDF environment is not only overdense with respect to the average, but also to the galaxy number density around other Y105 ∼ 26 galaxies at the same redshift, that show Lyα emission only in ∼15% of the cases. However, the only other field in Pentericci et al. (2014) where imaging data of comparable depth are available is GOODS-South: interestingly, we verified that all three galaxies with Y105 < 26.5 in this field lack both Lyα and any significant overdensity around them. Given the limitation of available data in constraining the proposed scenario, we carry out a more in-depth evaluation through our cosmological simulations (Hutter et al. 2014, 2015) that model both the overall reionization process and the UV and Lyα emission properties of $z \simeq 7$ galaxies.

4.1. Comparison with an SPH Theoretical Model

The model couples cosmological SPH simulations run using GADGET-2 (Springel 2005) with a radiative transfer code (pCRASH, Partl et al. 2011) and a dust model. We explore a wide range of $f_{\rm esc}$, ranging between 5%–95%. For each of these values, we couple the $z \sim 7$ simulation snapshot with pCRASH, starting from a fully neutral IGM and ending the runs once the IGM is fully ionized. We look for galaxies resembling BDF-521 and BDF-3299 in terms of Lyα and UV luminosity in a snapshot with an average neutral fraction $\langle \chi_{\rm H\,I} \rangle \simeq 0.5$ consistent with current estimates at $z \sim 7$ (Bouwens et al. 2015b; Mitra et al. 2015). We take $f_{\rm esc} = 0.5$ as the reference ionizing escape fraction. However, our analysis is unaffected by the $f_{\rm esc}$ value adopted: as shown in Hutter et al. (2014, 2015) the visibility of LAEs is governed by three degenerate quantities, $f_{\rm esc}$, $\langle \chi_{\rm H\,I} \rangle$ and the dust absorption; at a given $\langle \chi_{\rm H\,I} \rangle$, a lower (higher) $f_{\rm esc}$ could be compensated by a lower (higher) dust absorption, mostly leaving both the reionization topology and the fraction of LAEs unchanged. Our simulation contains 75 sub-volumes equal to the observed one: we find 7 (10) LAEs that match the Lyα and UV ranges of BDF-521 (BDF-3299), but only *two pairs* that are at comparable distances (∼4 pMpc), implying that the existence of such "clustered pairs" is rare, with a probability of only about 2.6%. This value is roughly consistent with current findings, the BDF emitters being the only pair found among 68 z-dropout galaxies surveyed by Pentericci et al. (2014). We compute the galaxy density and the average neutral fraction in regions equivalent to one *HST* pointing around the two pairs and compare them with values measured around isolated LAEs and normal LBGs in the model (Figure 4). We find that both "clustered pairs" lie in *highly ionized regions* and are characterized by a *significant clustering* of LBGs in their surroundings. In general, there is an evident relation between the neutral hydrogen fraction and the galaxy density at $\chi_{\rm H\,I} > 0.1$. Model LAEs are found at $\chi_{\rm H\,I} \lesssim 0.1$, with clustered LAEs being embedded in overdense regions with a very low neutral H I fraction of $\log(\chi_{\rm H\,I}) \sim -5$. By inspecting the LBG populations surrounding the "clustered pairs," we find that the first pair shows LBG number counts that are very similar to the BDF observed ones (green line in Figure 3), while the second group shows an LBG overdensity at $Y \gtrsim 28$, fainter than the BDF limiting magnitude. A snapshot of Pair 1 from the model is shown in Figure 5: the LAEs and companion LBGs lie in an ionized region with a radius of about ≃5 pMpc, where $\chi_{\rm H\,I}$ increases from 10^{-6} to 10^{-3} up to a sharp transition boundary with the mostly neutral IGM. This lends support to

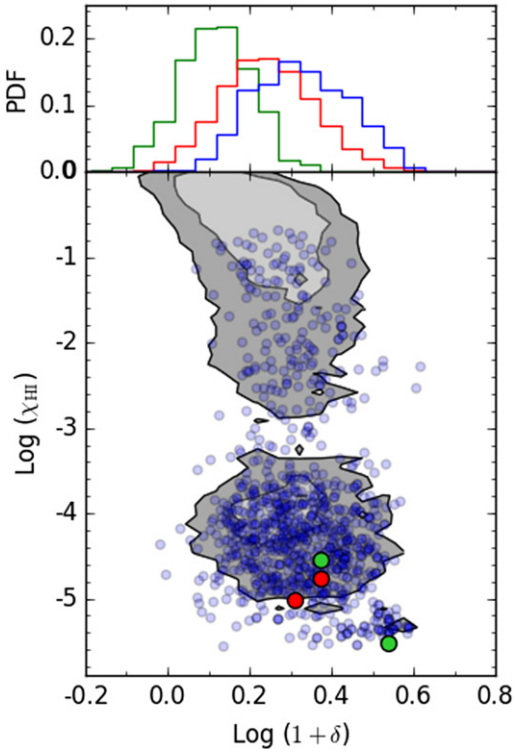

Figure 4. Bottom panel: hydrogen neutral fraction versus galaxy overdensity in our cosmological simulations. Gray contours show the region occupied by LBGs, blue circles mark the position of LAEs. The LAEs in "clustered pairs" are shown in green (Pair 1) and red (Pair 2). Top panel: density distribution of the LAEs (blue) and of the LBGs in regions with hydrogen neutral fraction above (red) and below (green) the average $\chi_{\rm H\,I} = 0.5$.

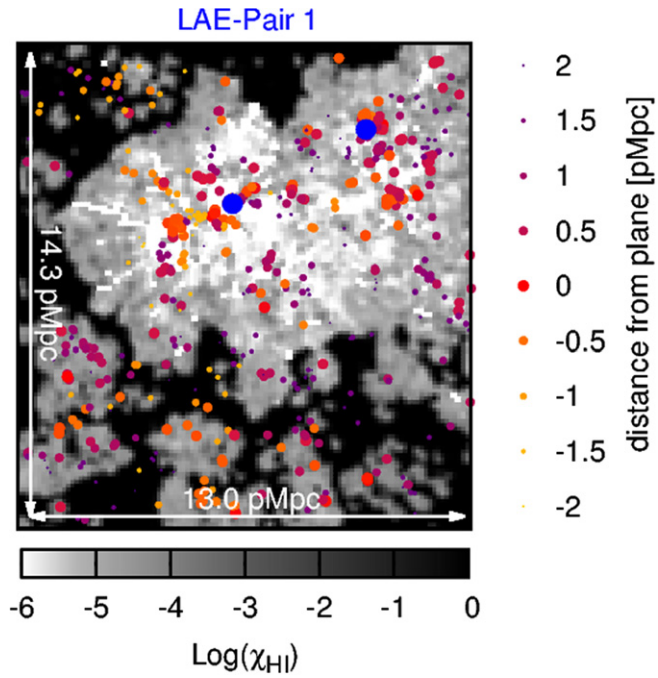

Figure 5. "Pair 1" region in the model with main LAEs (blue circles) and their companion LBGs shown as circles with color and dimension indicating the distance from the displayed plane.

our suggestion that the BDF field hosts an early reionized region pointing to a connection between galaxy clustering and the reionization timeline.

5. SUMMARY AND CONCLUSIONS

The analysis of dedicated *HST* observations has shown that the BDF field, where we previously detected a unique pair of Lyα emitting galaxies at $z \sim 7$ (Vanzella et al. 2011), presents a number density of $z \sim 7$ LBGs, which is larger by a factor of approximately three to four than the average one. A comparison between observations and cosmological simulations shows that the BDF likely hosts overlapping reionized regions with a very low neutral fraction ($\chi_{\rm H\,I} < 10^{-3}$) embedded in a half neutral IGM. Our findings match the expectation that overdense regions are the first to become reionized, and suggest that source clustering is a likely explanation for the inhomogeneity of reionization measured from spectroscopy (Pentericci et al. 2014). Finally, the consistency with model predictions on the relation between clustering and the neutral hydrogen fraction, adds further evidence to a scenario where faint star-forming galaxies play a major role in reionization (Bouwens et al. 2015a). This picture clearly highlights the potentiality of going beyond the standard approach based on volume-averaged quantities, and investigating instead the properties of the ionizing and Lyα-emitting sources as a function of different environments in order to constrain the unfolding of the reionization epoch.

Based on observations made with the NASA/ESA *Hubble Space Telescope*, obtained at the Space Telescope Science Institute, which is operated by the Association of Universities for Research in Astronomy, Inc., under NASA contract NAS 5-26555. These observations are associated with program #13688. The research leading to these results has received funding from the European Union Seventh Framework Programme (FP7/2007–2013) under grant agreement n 312725.

REFERENCES

Bertin, E., & Arnouts, S. 1996, A&AS, 117, 393
Bouwens, R. J., Illingworth, G. D., Oesch, P. A., et al. 2015a, ApJ, 811, 140
Bouwens, R. J., Illingworth, G. D., Oesch, P. A., et al. 2015b, ApJ, 803, 34
Brammer, G., Pirzkal, N., McCullough, P., & MacKenty, J. 2014, Time-varying Excess Earth-glow Backgrounds in the WFC3/IR Channel, Tech. rep. (Baltimore, MD: STScI)
Bruzual, G., & Charlot, S. 2003, MNRAS, 344, 1000
Cai, Z., Fan, X., Jiang, L., et al. 2015, ApJL, 799, L19
Calzetti, D., Armus, L., Bohlin, R. C., et al. 2000, ApJ, 533, 682
Caruana, J., Bunker, A. J., Wilkins, S. M., et al. 2012, MNRAS, 427, 3055
Castellano, M., Fontana, A., Boutsia, K., et al. 2010a, A&A, 511, A20
Castellano, M., Fontana, A., Grazian, A., et al. 2012, A&A, 540, A39
Castellano, M., Fontana, A., Paris, D., et al. 2010b, A&A, 524, A28
Castellano, M., Sommariva, V., Fontana, A., et al. 2014, A&A, 566, A19
Dayal, P., Ferrara, A., Saro, A., et al. 2009, MNRAS, 400, 2000
Dijkstra, M. 2016, in Understanding the Epoch of Cosmic Reionization, ed. A. Mesinger (Astrophysics and Space Science Library, Vol. 423; Cham, Switzerland: Springer International), 145
Finkelstein, S. L., Ryan, R. E., Jr., Papovich, C., et al. 2015, ApJ, 810, 71
Fontana, A., D'Odorico, S., Poli, F., et al. 2000, AJ, 120, 2206
Fontana, A., Dunlop, J. S., Paris, D., et al. 2014, A&A, 570, A11
Fontana, A., Vanzella, E., Pentericci, L., et al. 2010, ApJL, 725, L205
Gonzaga, S., Hack, W., Fruchter, A., & Mack, J. 2012, The DrizzlePac Handbook (Baltimore, MD: STScI)
Grazian, A., Castellano, M., Fontana, A., et al. 2012, A&A, 547, A51
Guo, Y., Ferguson, H. C., Giavalisco, M., et al. 2013, ApJS, 207, 24
Hutter, A., Dayal, P., & Müller, V. 2015, MNRAS, 450, 4025
Hutter, A., Dayal, P., Partl, A. M., & Müller, V. 2014, MNRAS, 441, 2861
Iliev, I. T., Mellema, G., Ahn, K., et al. 2014, MNRAS, 439, 725
Koekemoer, A. M., Ellis, R. S., McLure, R. J., et al. 2013, ApJS, 209, 3
Loeb, A., Barkana, R., & Hernquist, L. 2005, ApJ, 620, 553

McQuinn, M., Lidz, A., Zahn, O., et al. 2007, MNRAS, 377, 1043
Merlin, E., Fontana, A., Ferguson, H. C., et al. 2015, A&A, 582, A15
Mitra, S., Choudhury, T. R., & Ferrara, A. 2015, MNRAS, 454, L76
Momcheva, I. G., Brammer, G. B., van Dokkum, P. G., et al. 2015, ApJS, submitted (arXiv:1510.02106)
Ono, Y., Ouchi, M., Mobasher, B., et al. 2012, ApJ, 744, 83
Partl, A. M., Maselli, A., Ciardi, B., Ferrara, A., & Müller, V. 2011, MNRAS, 414, 428
Pentericci, L., Fontana, A., Vanzella, E., et al. 2011, ApJ, 743, 132
Pentericci, L., Vanzella, E., Fontana, A., et al. 2014, ApJ, 793, 113
Schaerer, D., & de Barros, S. 2009, A&A, 502, 423
Schenker, M. A., Stark, D. P., Ellis, R. S., et al. 2012, ApJ, 744, 179
Springel, V. 2005, MNRAS, 364, 1105
Stark, D. P., Ellis, R. S., Chiu, K., Ouchi, M., & Bunker, A. 2010, MNRAS, 408, 1628
Trenti, M., & Stiavelli, M. 2008, ApJ, 676, 767
Treu, T., Trenti, M., Stiavelli, M., Auger, M. W., & Bradley, L. D. 2012, ApJ, 747, 27
Vanzella, E., Fontana, A., Zitrin, A., et al. 2014, ApJL, 783, L12
Vanzella, E., Pentericci, L., Fontana, A., et al. 2011, ApJL, 730, L35
Wyithe, J. S. B., & Loeb, A. 2005, ApJ, 625, 1
Wyithe, J. S. B., & Loeb, A. 2007, MNRAS, 382, 921